Sustainable Materials and Technologies 45 (2025) e01541

Contents lists available at ScienceDirect

Sustainable Materials and Technologies

journal homepage: www.elsevier.com/locate/susmat

Preliminary assessment of alkali-resistant flax based meshes for reinforcing cementitious composites

Jaka Gašper Pečnik [a,b,*], Laetitia Marrot [c], Marica Mikuljan [a], Tania Langella [a], Matthew Schwarzkopf [a,b]

[a] InnoRenew CoE, Livade 6a, 6310 Izola, Slovenia
[b] University of Primorska, Titov Trg 4, 6000 Koper, Slovenia
[c] Slovenian National Building and Civil Engineering Institute (ZAG), Dimičeva 12, 1000 Ljubljana, Slovenia

ARTICLE INFO

Keywords:
Flax
Flax based meshes
Grid
TRC
Cementitious composites
Mesh mechanical properties
Pull-out
Bond strength
Durability

ABSTRACT

The production of textile-reinforced concrete (TRC) requires less materials and energy in comparison with conventional concrete reinforced with steel rebars, which draws some solutions towards the production of net zero concrete that the Cement and Concrete Industry sector should reach by 2050. To go one step further, this study investigates the development of flax based meshes as basic components for a reinforcement grid in cementitious materials. Flax strands and hybrid strands (combination of flax strands and glass or basalt rovings) were impregnated with an epoxy resin to form meshes. The physical and mechanical properties of the flax based meshes were assessed and the alkaline resistance of these reinforcing materials was evaluated to determine their durability in a cementitious matrix. At isoweight of reinforcement, the flax-based meshes demonstrated the best performance in terms of specific modulus and specific strength compared to the hybrid meshes. The hybrid meshes from the control batch displayed specific properties in the same range, whether they were constituted of AR-glass or basalt. However, the use of alkali-resistant glass rovings strongly mitigated the degradation of the mechanical properties of the hybrids meshes by making them less affected by the alkaline environment, among all the reinforcement meshes. In contrast, hybrid meshes with basalt experienced an extensive reduction in tensile strength and strain after exposure to alkaline environment, due to the corrosion of the basalt fibres. Pull-out tests revealed maximum bond strengths for the flax based meshes embedded in a high-performance concrete matrix.

1. Introduction

According to the Global Cement and Concrete Association, concrete is responsible for approximately 7 % of global CO_2 emissions [1]. The Cement and Concrete Industry is committed to achieving net-zero concrete production by 2050 and has developed a roadmap outlining the pathway to this goal. Among the identified contributions, efficiency in design and construction account for 22 %, and 9 % stems from savings in cement and binders [1]. Indeed, the concrete industry is one of the major consumers of natural resources, and the increasing production of concrete has heavily solicited the natural reserve of these resources [2].

In addition to environmental concerns, concrete has several limitations such as low tensile strength, brittleness, susceptibility to early cracking (due to heat of hydration), and structural crack formation prior to loading caused by drying shrinkage or other volume changes [3]. To improve properties of concrete under tensile loading conditions (e.g. bending), a complementary supporting material is required to absorb excessive tensile forces. Textile-reinforced concrete (TRC) first appeared in the 70s and has since been recognised as a high potential construction material [4,5]. It consists of a cementitious matrix reinforced by non-metallic mesh-like fabrics that can be made from various types of fibres. The main advantage of TRC is its sustainability, particularly in terms of raw material usage (TRC cross section is lower than 50 mm) in comparison with a conventional concrete construction (cross sections of 100–300 mm) [6]. TRC does not require an additional concrete layer to protect steel from corrosion as textile or grid reinforcement are non-corrosive. The reduction in material requirement lowers energy consumption, carbon footprint [6], and overall material costs.

Various studies have explored the use of carbon [7], glass [8], and to a lesser extent, basalt [9] fibre reinforcements. As a more sustainable

* Corresponding author at: InnoRenew CoE, Livade 6a, 6310 Izola, Slovenia.
E-mail address: jaka.pecnik@innorenew.eu (J.G. Pečnik).

https://doi.org/10.1016/j.susmat.2025.e01541
Received 21 January 2025; Received in revised form 26 May 2025; Accepted 13 July 2025
Available online 17 July 2025

alternative, plant fibres are widely available in most countries and offer a cost-effective, low density reinforcement material. In addition, plant fibres are biodegradable, renewable, non-hazardous and non-abrasive. Among plant fibres, flax fibres exhibit superior tensile properties, comparable to alpha and ramie fibres [10]. Flax fibres in particular, have specific mechanical properties (i.e. specific strength and modulus) that are comparable to those of glass fibres, which make the plant interesting for the reinforcement of cement-based materials [10]. Several studies have reported the use of plant fibres —such as hemp [11–13], flax [14], jute [15]—for making fabrics and grids to reinforce cement-based matrices. However, studies involving a vegetal grid-type reinforcement [11,16] remain limited due to the unavailability of such product.

During hardening, cement-based matrices exhibit a highly alkaline environment (pH 12.5–13.5) due to hydration products such as calcium hydroxide and alkalis. This alkaline environment can be aggressive to fibrous reinforcement and, over time, can considerably affect the durability of the composites. For example, the sensitivity of *E*-glass fibres to alkaline environment led to the development of alkali-resistant (AR) glass fibres, the composition of which was optimised (by adding zirconia) for use in composite material products incorporating Portland cement. Similarly, plant fibres are weakened by an alkaline environment due to the dissolution of lignin and hemicellulose components, alkaline hydrolysis of the cellulose molecules, and mineralisation caused by the migration of hydration products into the lumens, along with volume variation [17,18]. To address these challenges and enable the effective use of plant fibres as reinforcement in cementitious matrices, two approaches can be considered: reducing the alkalinity of the cement by partially replacing the Portland cement with pozzolanic materials (e.g. metakaolin, fly ash, silica fume) [17,18], or applying an adequate coating to protect the fibres in a conventional cementitious matrix. In addition to protecting against chemical attack, coatings and sizing of fibrous reinforcement have several roles: i) increasing the strength of the fibres by providing a healing effect for surface flaws, ii) binding the filaments together and allowing them to carry the load as a single unit, iii) improving the adhesion between fabric and cementitious matrix, conferring more efficient stress propagation between the filaments and the matrix, and iv) providing additional structure for easier handling and alignment of the reinforcement in the cementitious matrix during manufacturing.

This study investigated the development of sustainable and alkali-resistant meshes as basic components of a grid tailored for reinforcing cementitious matrices. AR-glass was selected as reference material due to its well-established application as reinforcement in cementitious matrices for construction and civil engineering since the late 1960s [19]. Basalt roving was selected as natural reinforcement for its higher tensile properties than glass [20] while being more eco-friendly than carbon due to the natural abundance of basalt rocks. Flax was selected due to its superior performance in reinforcement among the plant fibres, its environmental sustainability, and the potential for reducing carbon footprints in construction materials. A few available studies highlighted a reduced environmental impact when replacing synthetic fibres (i.e. glass and polyacrylonitrile fibres) by plant fibres to reinforce cementitious products [21,22]. The flax based meshes were composed either of flax strands or a combination of flax strands and synthetic (glass and basalt) rovings, referred to as hybrid strands. Including hybrid strands was intended to enhance the sustainability of purely synthetic reinforcements, while compensating for the potential loss in the performance of flax strands when exposed to an alkaline environment within a cementitious matrix. The strands were impregnated by an epoxy resin to form meshes. The objectives of this study were to: i) assess the physical and mechanical properties of the flax based meshes for reinforcing cementitious matrices, ii) evaluate the alkaline resistance of these reinforcing materials to determine their durability in a cementitious matrix, and iii) evaluate the bonding strength between the meshes and a high-performance concrete matrix.

2. Materials and methods

2.1. Materials

The characteristics of the flax strands and synthetic rovings used in the study are given in the Table 1. Two different flax strands were selected: one which did not undergo any treatment (untreated), and one which was bleached. Scouring and bleaching treatments, commonly applied during yarn production, modify the composition of flax by removing constituents, such as pectins, hemicelluloses and lignin, which influences the mechanical and morphological properties of flax [23].

A two-component epoxy resin Lamepox 23 (Samson Kamnik, Slovenia) (mixing ratio 100:23) was used for the impregnation of flax and hybrid strands (described in 2.2.2).

High-performance concrete served as cementitious matrix for the pull-out tests. The high-performance concrete mixture was prepared with Portland cement (CEM I 42.5R), technical silica sand, silica flour, silica fume, superplasticizers and water. The ratio of the components is given in Vlach et al. [24], and the cement – water ratio was taken at 0.25.

2.2. Methods

2.2.1. Preparation of hybrid strands

Hybrid strands were fabricated by twisting combinations of flax and synthetic rovings, as illustrated Fig. 1. The flax strands, together with alkali-resistant glass or basalt rovings were clamped on one end (a), passed through a sheath (b), and clamped separately to a spinning bar (c) to ensure a constant twisting angle of 120°. Twisting was performed with $n = 100{,}000$ *Z*-twists per 1000 m. The initial length of the strands before twisting was approximately 7 m.

2.2.2. Impregnation of flax and hybrid reinforcement strands

The flax and hybrid strands were impregnated with an epoxy resin in a vacuum chamber under the following conditions: 30 °C, 100 mbar, 60 min.

Impregnating the reinforcement strands in epoxy resin protects the strands against alkali attack, binds the two different materials in hybrid strands to enable them to carry the load as a single unit, and facilitates easier handling of the developed, flexible yet solid, grid for reinforcing the cementitious matrix.

In this study, the physical properties (linear density and density) of the non-impregnated flax and hybrid strands, and the impregnated flax and hybrid meshes will be investigated to better understand the effect of the fibre and matrix components. The mechanical properties and alkali resistance will then be evaluated only for the impregnated meshes, since they are considered the basic components of reinforcement grids.

All fibrous reinforcements (non-impregnated strands and impregnated meshes) are presented in Table 2, resulting in a total of 12 reinforcement groups.

After impregnation, the meshes were stretched between two bolts to dry at room temperature for one day, cut to 550 mm, and cured in the

Table 1
Characteristics of the flax and synthetic strands.

Material	Treatment	Type of strand	Provider	Sample ID
Flax	Untreated	Twine (3 threads)	Gepotex Inh. (Germany)	UFS
Flax	Bleached (White)	Twine (8 threads)	Juta a.s. (Czech Republic)	WFS
Basalt	–	Roving	CBG composite GmbH (Germany)	BR
AR-Glass	Alkali resistant	Roving	Fibre Technologies International Ltd. (United Kingdom)	ARGR

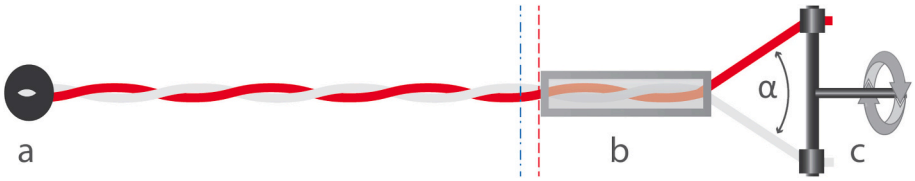

Fig. 1. Process of fabricating a hybrid reinforcement strand from flax strands and glass/basalt rovings by twisting process.

Table 2
Reinforcement groups (non-impregnated strands, and impregnated meshes).

Fibrous reinforcement	Impregnation matrix	Group ID	Physical properties	Mechanical properties	Alkali resistance	Pull-out test
Flax	None	UFS	x	–	–	–
	Epoxy	UFS-E	x	x	x	x
White flax	None	WFS	x	–	–	–
	Epoxy	WFS-E	x	x	x	x
Flax / AR-glass	None	UFS-ARGR	x	–	–	–
	Epoxy	UFS-ARGR-E	x	x	x	x
Flax / Basalt	None	UFS-BR	x	–	–	–
	Epoxy	UFS-BR-E	x	x	x	x
White flax / AR-glass	None	WFS-ARGR	x	–	–	–
	Epoxy	WFS-ARGR-E	x	x	x	x
White flax / Basalt	None	WFS-BR	x	–	–	–
	Epoxy	WFS-BR-E	x	x	x	x

oven at 125 °C for one hour. All impregnated meshes (20 repetitions per reinforcement group) were cut to a final length of 450 mm and placed in a climate chamber at 20 °C and 65 % relative humidity (RH) for 4 weeks to ensure that the resin was fully cured.

2.2.3. Physical properties of the flax and hybrid meshes

Mass of the reinforcement groups was measured on ten replicates. The mass M of a strand or mesh with a length L of 50 cm was measured with a (Mettler Toledo, USA) scale with a precision of 0.1 mg. The average linear density λ was calculated according to (1):

$$\lambda = M/L \times 1000 \quad (1)$$

With λ in g.km^{-1}, M in g and L in m.

The density in g/cm^3 of the strands was measured with a gas displacement AccuPyc II 1340 pycnometer (Micromeritic, USA) using research grade helium (5.0).

2.2.4. Alkaline exposure of the flax and hybrid meshes

The resistance of reinforcements to an alkaline environment in a cementitious matrix was evaluated with a protocol inspired from the standard ISO 10406-1:2015 (Fibre-reinforced polymer (FRP) reinforcement of concrete - Test methods). An alkaline solution (pH ~14) was prepared by adding 8.0 g NaOH and 22.4 g KOH to 1 L of distilled water. Ten replicates of each impregnated group of mesh were immersed in alkaline solution at ambient temperature (instead of 60 °C as required by the standard) for 60 days (instead of 30 days as required by the standard). At the end of the 60 days, the samples were carefully washed with water, dried first at room temperature and then oven dried at 60 °C for 24 h, and finally reconditioned in a climate chamber at 20 °C and 65 % RH until tensile testing.

2.2.5. Mechanical properties of the flax and hybrid meshes

The mechanical properties of flax and hybrid meshes that were not exposed to an alkaline environment (pre-alkali) served as the control group. The mechanical properties of flax and hybrid meshes from batches exposed to an alkaline environment (post alkali) were measured to assess any reduction in mechanical performance. Tensile tests were performed on a static, universal testing machine (Zwick Roell, Germany). Specimens were hydraulically clamped between two wooden blocks within the metal clamps to reduce potential damage to the strands and to reduce stress concentration in the clamps. The test span was 300 mm, at a test speed of 2 mm/min. Before starting the test, the meshes were preloaded at 20 N to increase the consistency of the results from one reinforcement group to the other. A minimum of seven valid tests per reinforcement group were recorded. The elastic modulus (E) was calculated between 0.1 and 0.3 % deformation. The maximum force and cross-sectional area were used to calculate maximum tensile strength (σ). Given the considerable influence of the cross-section determination on the calculations to determine the mechanical properties, two experimental methodologies were compared to measure the cross-sectional area.

Apparent diameter method – The apparent diameter of the strands was measured over a 15 mm length with a VHX-6000 digital microscope (Keyence, Belgium). An average of 10 measurements provided the apparent diameter d, which was then applied in (2), assuming a circular cross-section A of the meshes.

$$A = \pi(d/2)^2 \times 100 \quad (2)$$

With A in m^2 and d in m.

Fingerprint method – The meshes were cut by a microtome blade, the cross-sections were stained with a dye and stamped on paper, appearing as a "fingerprint". Dimensions of the stamp were measured with a VHX-6000 digital microscope (Keyence, Belgium). The coloured surface area was processed by the Digimizer image analysis software, counting squares with dimensions of 0.1 × 0.1 mm^2. An average of five measurements were used to determine cross-section. This method was also used to assess the circularity of the cross-section.

2.2.6. Preparation of embedded strands in high performance concrete and pull-out test

Pull-out tests were carried out to assess the bonding of the flax and hybrid reinforcements with a concrete matrix. For the six types of impregnated reinforcement groups (see Table 2), 5 meshes of approximately 15 cm long were embedded in concrete. To do so, plastic tubes (22.5 mm diameter, and 15 mm long) were placed on a supporting wooden board. 20 mm deep holes were drilled in the wooden board in the center of the plastic tubes. The meshes were positioned in the holes in upstanding position. Then, the high performance concrete mixture was poured into the plastic tubes, filling them entirely. Hence, the embedded length of the meshes was equal to the length of the tubes, i.e.

15 mm. Specimens were left drying at ambient temperature and rested at least 60 days prior to the pull-out tests.

Pull-out tests were conducted on a universal testing machine (Zwick Roell, Germany) with a 50 kN load cell at a testing speed of 2 mm/min. As illustrated Fig. 2, on the upper part of the testing machine, a steel frame with a grove cut was pressed between the hydrolic grips. The concrete cylinder was placed on the steel plate with the longer non-embedded part of the mesh facing downwards in the frame. The distance to the bottom grip was set 5 cm apart. Meshes specimens were hydraulically clamped in the lower grip between two wooden blocks to reduce potential damage to the strands and to reduce stress concentration in the clamps. Before starting the test, the meshes were preloaded at 20 N to increase the consistency of the results from one reinforcement group to the other. Force and displacement diagrams were recorded. The maximum pull out strength τ_{max} was calculated as the ratio of the maximum force F_{max} (in N) to the embedded surface (L_e describes the embedded length of the meshes and d the average mesh diameter) according to the eq. (3):

$$\tau_{max} = \frac{F_{max}}{\pi L_e d} \quad (3)$$

The average mesh diameter was calculated from the area given by the fingerprint method, assuming a circular area.

2.2.7. Statistical analyses

Data analyses from mechanical testing of the flax and hybrid meshes were conducted in R (4.5.0) using RStudio (version 2025.05.0 + 496). The measurements are reported as medians, Q1, Q3 and interquartile range (IQR). The Shapiro-Wilk normality test revealed a significant deviation from normality in the residuals. For that purpose, non-parametric Wilcoxon tests were conducted to examine differences in groups. A Wilcoxon rank sum test (Wilcoxon test) was assessed to check for significant differences between reinforcement as pre and post alkaline exposure for Youngs modulus, strength, and strain values. The outcome of the tests resulted with 95 % percent confidence interval (CI), sample estimates for the difference in location and *p*-values. The significance level was set at $\alpha = 0.05$.

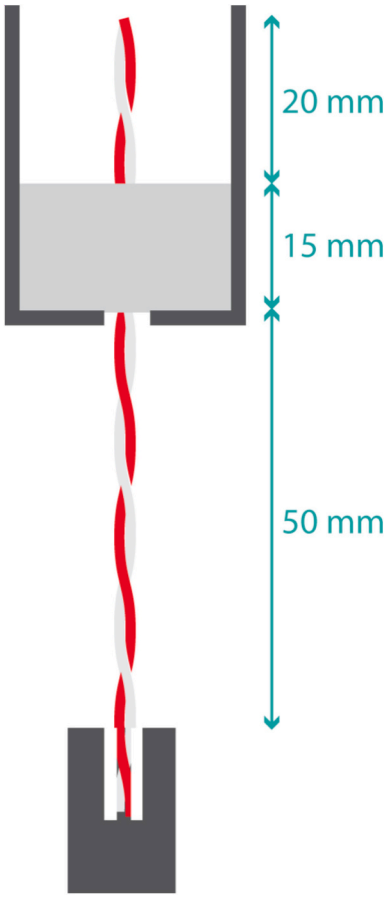

Fig. 2. Pull-out test setup.

3. Results & discussion

3.1. Physical properties of the reinforcement groups

The densities of the reinforcement groups presented in Fig. 3 shows that the density of the untreated flax strand (UFS) is 1.54 g/cm^3 and 1.69 g/cm^3 for the bleached strand (WFS). These values are in accordance with literature where the flax density is estimated to be ~1.5 g/cm^3, highlighting significant variations in the density depending on the experimental set up [25]. The two flax strands come from different producers, so the flax used in their composition is not the same. Flax variety, location, year of cultivation, maturity at harvest, retting type and duration, are among a list of factors that influence flax composition and the resulting density. Hence, the higher density observed for the bleached flax strands cannot be solely attributed to the bleaching treatment. The density of the synthetic fibres (2.63 g/cm^3 for basalt and 2.54 g/cm^3 for AR-glass rovings according to the providers' datasheet) are more than 50 % higher than the density of the flax strands. This underlines the need to consider linear density when calculating mechanical properties (investigated Section 3.2.2). Combining flax strands with synthetic rovings increased the overall density of the hybrid strands. The two highest densities were recorded for the two flax strands combined with basalt roving (UFS-BR and WFS-BR), as the basalt already had the highest density among the different materials used. Impregnating the strands decreased the density of the flax and hybrids strands since the density of epoxy (1.1 g/cm^3 according to the producer technical data sheet) is lower than the densities of flax, glass, or basalt.

The linear density of the reinforcement strands is presented in Fig. 4. Unlike density which compares groups at iso volume, linear density compares them at iso length. Indeed, there are substantial differences in the cross-section between different reinforcement groups (Section 3.2.2). Flax strands displayed the lowest linear density values compared to the synthetic AR-glass and basalt roving (both at 2400 g/km from the provider datasheet). The difference in linear density between the two flax strands is related to the linear density of their constitutive threads and to the number of threads in their twisted structure. Specifically, the linear density of the 3 constitutive threads of the untreated flax (UFS) was measured at 167 ± 22 g/km and the linear density of the 8 constitutive threads of the bleached flax was 102 ± 11 g/km. When combined with the synthetic rovings, for a given type of flax (i.e. untreated or bleached), the linear density of the hybrids (with basalt and AR-glass) is equivalent (linear densities of UFS-ARGR and UFS-BR were

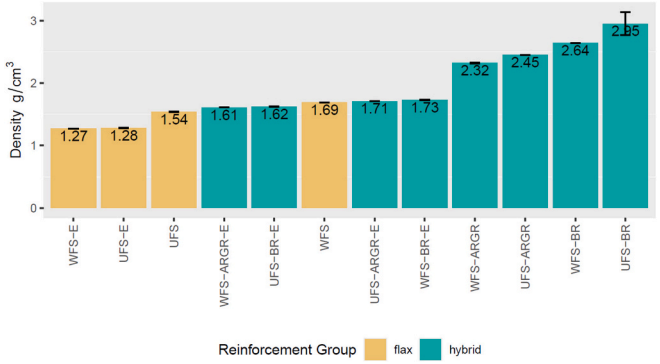

Fig. 3. Density of the reinforcement groups.

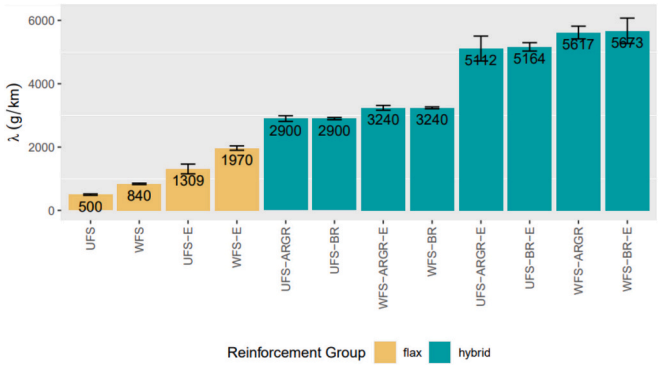

Fig. 4. Linear density of flax and hybrid reinforced strands.

2900 g/m^2, and linear densities of WFS-ARGR and WFS-BR were 3240 g/m^2), due to the equal linear density of the AR-glass and basalt roving. After impregnation in epoxy, the linear density of all combinations of reinforcements increased, due to the additional weight of the epoxy matrix on a given length. However, the linear density clearly increased for the flax strands (by 162 % and 135 % for the untreated and bleached group, respectively) compared to the hybrids (between 73 and 78 % for the two types of flax combined either with AR-glass or basalt). This observation can be attributed to the high absorption of the epoxy matrix by the flax strands and the chemical interactions between the epoxy and the hydroxyls groups at the surface of the flax fibres. Additionally, physical "entrapment" of the resin occurs due to several factors: (i) the rough surface of the flax fibres, (ii) the entangled network of flax fibres constituting the strands at the fibre scale, and (iii) the entangled network at the thread scale with the twined structure that creates more obstacles for the resin to leach. In contrast, the synthetic fibres are perfectly aligned within the roving, and their smooth surface offers little possibilities for retaining the epoxy matrix. Overall, the average linear density of the reinforcement groups spans from 500 to 5673 g/km (more than 11 times higher). Consequently, the associated cross-sectional area is expected to vary. Its accurate determination is crucial for the calculation of the mechanical performance of the reinforcements, which is the focus of the following section.

3.2. *Mechanical properties of the flax and hybrid meshes*

This section evaluates the mechanical properties and alkali resistance for the impregnated meshes only, since they are considered the basic components of a reinforcement grid.

3.2.1. *Cross-sectional area*

The cross-sectional area of the meshes was obtained by two different methods. Fig. 5 illustrates the principle of the first method consisting of measuring the apparent diameter of the meshes under digital microscope and Fig. 6 shows the images obtained by the second method using the fingerprint area. Cross-sectional area results are reported in Table 3.

For both methods, the standard deviation is low, and there are minor differences in the cross-sectional area between the two methods. As presented in Fig. 5, the apparent diameter method involves measuring the apparent diameter of the strand (observed transversely). However, in cases where the cross section is not circular, this method tends to underestimate the real cross-sectional area because the sample typically rests on its flatter surface. The lower values between the two methods are highlighted in bold in Table 3, and they are equally distributed between the two methods, suggesting that the cross-section is of a circular shape of. However, the images obtained by the fingerprint method (Fig. 6) reveal the irregular shape of the cross section of the hybrid mesh. Hence, for comparing the mechanical properties in Section 3.2.2, the cross-sectional area values obtained by the fingerprint method, considered as more accurate, were used for calculating the tensile strength and Young's modulus.

3.2.2. *Tensile properties pre- and post-alkaline exposure*

The tensile curves of each group of mesh, without alkaline exposure as control (pre), and after exposure to the alkaline environment (post) are presented in Fig. 7. Abrupt brittle break was the typical failure in most of the meshes, pre- and post-alkaline exposure.

Young's modulus E, tensile strength at break σ, and strain at failure ε_u of each group of meshes are reported in Tables 4–6 including median, 1st quartile (Q1), 3rd quartile (Q3), interquartile range (IQR), the difference (Δ) between the medians of pre and post tests, as well as the statistics according to the Wilcoxon test: W is the test statistic for the Wilcoxon test, p-value (α = 0.05), lower and upper values of the confidence interval (CI), and the difference in location.

For control batches, the flax mesh displayed the lowest Young modulus and strength at break, which can be explained by three factors: i) at the single fibre scale, tensile properties of glass fibres (E_{glass} = 76 GPa, σ_{glass} = 1400–2500 MPa [26]) and basalt fibres (E_{basalt} = 89 GPa, σ_{basalt} = 2800 MPa [26]) are superior to those of flax fibres (E_{flax} = 39.3 GPa, σ_{flax} = 700 MPa [27]), ii) the linear density of UFS-E and WFS-E are 3.9 and 2.9 times smaller than the density of their glass and basalt hybrids, respectively, iii) for the given linear density, the weight percentage of reinforcement is higher for hybrids than for the flax mesh, because of the high absorption of the epoxy matrix by the flax strands, as explained in Section 3.1. The elongation at break of the flax reinforcements stands between 1.6 and 2.2 % (Table 6). Since the literature reports elongation at break of glass and basalt fibres at 1.8–3.2 and

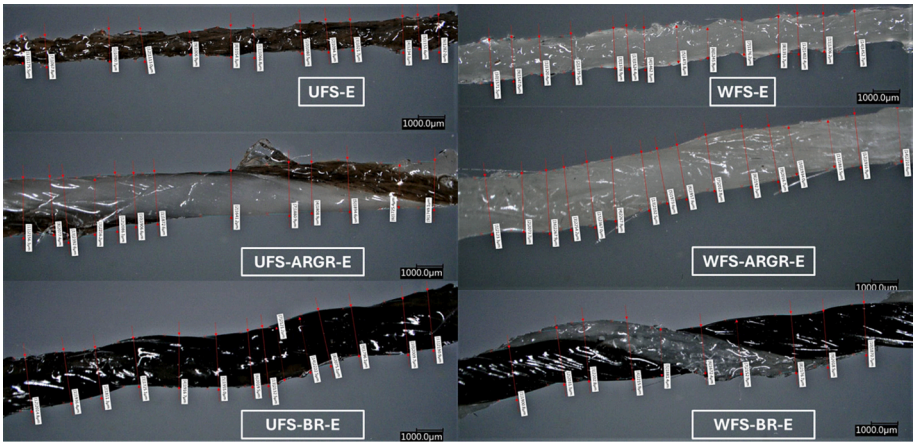

Fig. 5. Cross sectional area measured by the apparent diameter method.

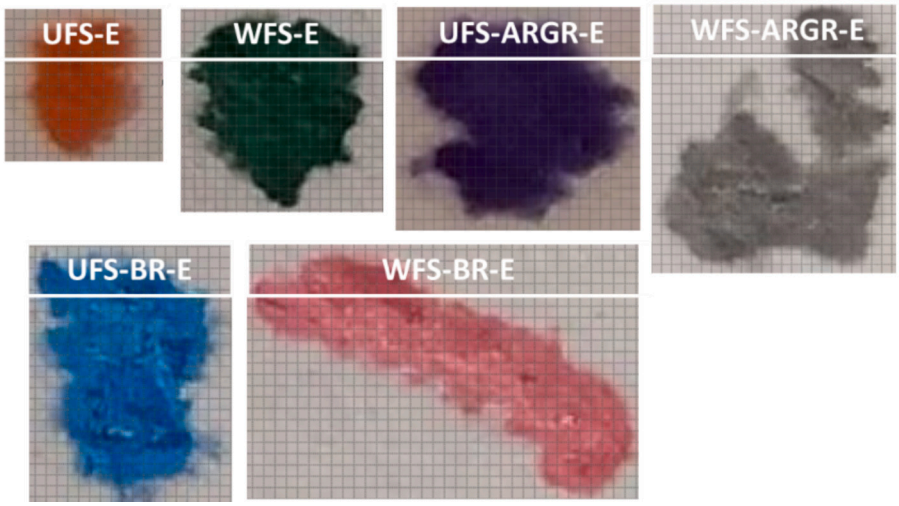

Fig. 6. Cross sectional area measured by the fingerprint method.

Table 3
Cross-sectional areas from the apparent diameter and fingerprint area methods, with lower values shown in bold.

Sample ID	Apparent diameter method	Fingerprint method
	$A_{app\ d}$ (m^2)	A_{fp} (m^2)
UFS-E	$\mathbf{0.98 \times 10^{-6} \pm 0.01 \times 10^{-6}}$	$1.00 \times 10^{-6} \pm 0.00 \times 10^{-6}$
WFS-E	$1.55 \times 10^{-6} \pm 0.01 \times 10^{-6}$	$1.55 \times 10^{-6} \pm 0.01 \times 10^{-6}$
UFS-ARGR-E	$3.01 \times 10^{-6} \pm 0.04 \times 10^{-6}$	$\mathbf{2.99 \times 10^{-6} \pm 0.01 \times 10^{-6}}$
UFS-BR-E	$3.21 \times 10^{-6} \pm 0.02 \times 10^{-6}$	$\mathbf{3.19 \times 10^{-6} \pm 0.01 \times 10^{-6}}$
WFS-ARGR-E	$\mathbf{3.49 \times 10^{-6} \pm 0.02 \times 10^{-6}}$	$3.50 \times 10^{-6} \pm 0.02 \times 10^{-6}$
WFS-BR-E	$\mathbf{3.16 \times 10^{-6} \pm 0.03 \times 10^{-6}}$	$3.29 \times 10^{-6} \pm 0.01 \times 10^{-6}$

3.15 %, respectively [26], and the elongation of epoxy matrices is higher than 3 % [28], it is likely that the breakage of the hybrids that occur between 1.6 and 2.0 % (Table 6), is precipitated by the breakage of the flax strands. Statistical analyses using the Wilcoxon rank sum test confirmed that, although for a small magnitude, significant differences (p-value <0.05) within the strain values pre and post alkaline exposure were observed for the groups: WFS-E, UFS-E, WFS-BR-E and UFS-BR-E (see Table 6). Significant differences in Young's modulus between groups pre and post alkaline treatment were found for 4 out of 6 subsets: WFS-E, UFS-E, UFS-BR-E and UFS-ARGR-E (Table 4). Finally, strength rank sum tests indicated significant differences in strength values between alkaline processes in 4 out of 6 reinforcements groups: WFS-E, UFS-E, WFS-BR-E and UFS-BR-E (Table 5).

The Young's modulus and tensile strength of all the hybrid combinations are close, ranging between 18.4 and 20.9 GPa (Table 4) and 278–361 MPa (Table 5), respectively. Despite the higher tensile properties of WFS-E compared to UFS-E, the hybrids combined with UFS demonstrated greater performance with a lower interquartile range than the ones combined with WFS. This can be attributed to the more irregular cross-section of WFS-ARGR-E and WFS-BR-E (see Fig. 6) due to the larger cross-section of WFS. The imposed torsion during hybrid fabrication might cause deformation of the rovings and create pressure zones during the tensile test, which could weaken the meshes.

After exposure to the alkaline environment, the hybrid batches made with AR-glass fibres were less affected. For both UFS-ARGR-E and WFS-ARGR-E, the Young's modulus decreased slightly (ΔE = 4–5 %, see Table 4). The tensile strength did not alter for UFS-ARGR-E and showed a small decrease for WFS-ARGR-E ($\Delta\sigma$ = 14 %). Amaro et al. [29] reported a significant decrease (−22 %) in the flexural strength of glass/epoxy composites that were exposed for 36 days in sodium hydroxide at pH 13. They attributed this to the micro-cracks in the epoxy due to the

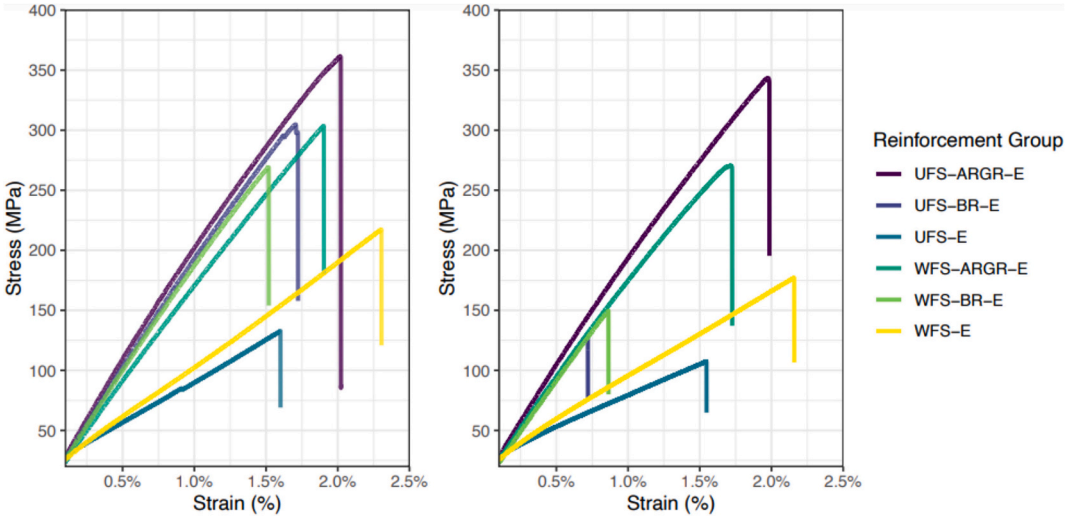

Fig. 7. Tensile curves of each group of mesh, without alkaline exposure as reference (pre-, on the left), and after exposure to the alkaline environment (post-, on the right).

Table 4
Young's modulus (E) of each reinforcement group for reference (pre) and exposed to the alkaline environment (post).

E (GPa)	*Pre*				*Post*				*Difference between pre and post treatment*					
Group	*Median*	Q_1	Q_3	*IQR*	*Median*	Q_1	Q_3	*IQR*	*ΔE*	*W*	*p-value*	*CI low*	*CI up*	*Diff in location*
UFS-E	8.0	7.1	8.5	1.4	6.6	6.4	7.1	0.8	18 %	76	0.010	127.2	760.1	425.9
WFS-E	9.5	9.3	9.6	0.3	9.1	8.9	9.2	0.3	4 %	78	0.006	345.2	2037.4	1203.5
UFS-ARGR-E	20.9	20.8	21.1	0.3	19.8	19.3	20.2	0.9	5 %	24	1.000	−3359.3	1853.2	−43.9
WFS-ARGR-E	18.4	17.2	18.7	1.5	17.6	17.2	17.8	0.6	4 %	66	0.021	114.5	2358.3	1522.7
UFS-BR-E	19.7	19.2	20.2	0.9	18.1	17.6	18.8	1.2	8 %	49	0.460	−887.7	1555.1	689.5
WFS-BR-E	18.4	17.0	19.2	2.2	17.6	17.2	19.1	1.9	5 %	72	0.028	399.1	1638.7	1043.6

Table 5
Tensile strength values (σ) of each reinforcement group for reference (pre) and exposed to the alkaline environment (post).

σ (Mpa)	*Pre*				*Post*				*Difference between pre and post treatment*					
Group	*median*	Q_1	Q_3	*IQR*	*median*	Q_1	Q_3	*IQR*	*Δσ*	*W*	*p-value*	*CI low*	*CI up*	*Diff in location*
UFS-E	147.0	132.6	160.2	27.6	109.5	104.2	112.4	8.3	26 %	90	0.000	23.0	49.0	38.4
WFS-E	217.2	205.2	221.8	16.7	175.8	172.9	182.2	9.3	19 %	89	0.000	21.1	52.8	35.7
UFS-ARGR-E	361.3	315.2	387.4	72.2	360.8	325.8	379.7	53.9	0 %	46	0.040	1.3	247.1	136.6
WFS-ARGR-E	317.3	264.2	344.1	79.9	273.0	239.5	282.1	42.6	14 %	80	0.000	150.8	218.0	185.2
UFS-BR-E	315.0	297.2	345.4	48.2	136.2	102.9	153.1	50.2	57 %	56	0.173	−21.5	102.6	46.2
WFS-BR-E	277.6	208.5	340.9	132.3	134.8	130.6	144.1	13.5	51 %	44	0.968	−60.9	39.1	−1.9

Table 6
Strain at failure values (εu) of each reinforcement group for reference (pre) and exposed to the alkaline environment (post).

ε_u (%)	*Pre*				*Post*				*Difference between pre and post treatment*					
Group	*median*	Q_1	Q_3	*IQR*	*median*	Q_1	Q_3	*IQR*	*Δ* ε_u	*W*	*p-value*	*CI low*	*CI up*	*Diff in location*
UFS-E	1.6 %	1.5 %	1.7 %	0.2 %	1.4 %	1.3 %	1.5 %	0.1 %	11 %	83	0.001	0.11 %	0.33 %	0.21 %
WFS-E	2.2 %	2.2 %	2.3 %	0.2 %	2.0 %	2.0 %	2.0 %	0.1 %	10 %	76	0.010	0.05 %	0.33 %	0.19 %
UFS-ARGR-E	2.0 %	1.7 %	2.1 %	0.4 %	2.0 %	1.7 %	2.0 %	0.3 %	1 %	49	0.014	0.10 %	1.41 %	0.80 %
WFS-ARGR-E	1.9 %	1.6 %	2.2 %	0.6 %	1.7 %	1.6 %	1.8 %	0.2 %	6 %	80	0.000	0.89 %	1.19 %	1.06 %
UFS-BR-E	1.7 %	1.7 %	1.9 %	0.2 %	0.7 %	0.6 %	0.8 %	0.2 %	58 %	50	0.408	−0.25 %	0.57 %	0.12 %
WFS-BR-E	1.6 %	1.2 %	2.0 %	0.7 %	0.8 %	0.7 %	0.8 %	0.1 %	49 %	50	0.720	−0.32 %	0.16 %	0.02 %

absorption of the solution by the matrix, leading to expansion and cracking, and subsequent exposure of the fibres as a consequence of the matrix dissolving in the solution [29]. In this study, the use of alkali-resistant glass roving effectively limited the degradation of the mechanical properties of the hybrid meshes.

Regarding the flax meshes, UFS-E showed greater loss of mechanical properties compared to WFS-E ($\Delta E = -18$ % and $\Delta\sigma = -26$ % for UFS-E, vs $\Delta E = -4$ % and $\Delta\sigma = -19$ % for WFS-E). In addition, the tensile strain decreased in both cases between 10 and 11 %. Besides the epoxy the flax fibres are also degraded by the alkaline environment through different mechanisms (dissolution and hydrolysis of their components, mineralisation and volume variation [17,30]), which lower the performance of flax based mesh. However, since the WFS received a bleaching treatment, part of its constituents (pectins, hemicelluloses and lignin) was already removed prior to the alkaline exposure, which explains why the WFS-E was less affected than UFS-E, which likely lost a higher proportion of components during the exposure.

Hybrid meshes with basalt (UFS-BR-E and WFS-BR-E) experienced an extensive reduction in tensile strength after exposure to alkaline environment, resulting in lowered values of 57 % and 51 % respectively, together with the highest reduction in tensile strain ($\Delta\varepsilon_u = -58$ and -49 %, respectively). Liu et al. [31] investigated the long-term alkali resistance of basalt fibres in benchmark cement supernatant as alkaline solution and observed a severe corrosion of the basalt fibres. Indeed, the chemical components of basalt fibres (silicate-based fibre) are predominantly SiO_2 (50–53 %) and Al_2O_3 (16–20 %), as well as other oxides in lower proportions: 5–10 % for CaO, MgO, Fe_2O_3 and Na_2O, and less than 5 % of K_2O [31]. The primary structure of the basalt fibres consist of networks composed of silicon-oxygen tetrahedra SiO_4^{4-}, aluminum-oxygen tetrahedra, and aluminum-oxygen octahedra [32]. Under an alkali attack, the hydroxydes OH^- degrade the Si—O and Al—O bonds within basalt fibres, disrupting the fibre's skeletal network structure [31]. Liu et al. [31] could follow this degradation by the evolution of the stretching vibrations of Si-O-Si and Al-O-Al on Fourier Transform Infra-Red spectra, and the gradual apparition of erosion pits on the fibre surface observed by scanning electron microscopy, associated with a decrease of their mechanical properties. The authors [31] highlighted the need to enhance the alkali resistance of basalt fibres when used in cementitious materials, which was confirmed by the results of this study. The corrosion pits are likely responsible for the premature rupture of the hybrid basalt meshes, without having a noticeable influence on the Young's modulus.

As highlighted in Section 3.1, the linear density varies among reinforcement groups, ranging from 1309 g/km for the UFS-E group to 5673 g/km for the WFS-BR-E group (a factor of 4). For a fairer comparison of reinforcements at iso weight, the specific modulus, defined as the Young's modulus divided by the linear density, and specific tensile strength, defined as the tensile strength divided by the linear density, are presented in Figs. 8 and 9 respectively.

At isoweight, the flax-based meshes, UFS-E and WFS-E, provide the best performance in terms of specific modulus and specific strength at break. The untreated UFS-E control outperformed the WFS-E control. However, after alkaline exposure, the specific tensile mechanical properties were close for both flax-based meshes, due to the greater performance loss in untreated flax. At isoweight, specific properties for the hybrid meshes from the control batches were in the same range, whether if they were constituted of AR-glass or basalt. The higher linear density of WFS resulted in hybrid meshes with a more irregular cross-section and potentially over stressed weak zones. Consequently, at isoweight, the UFS hybrids with glass and basalt displayed slightly higher specific

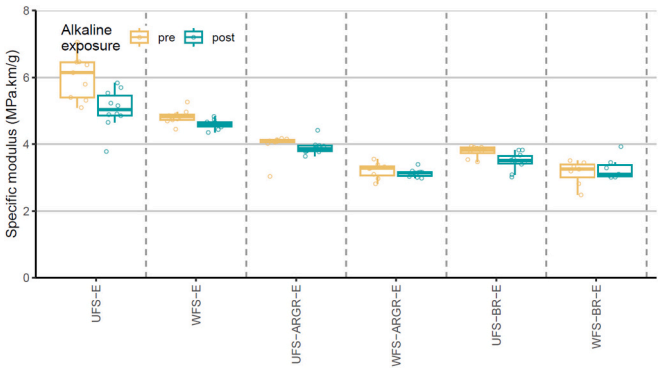

Fig. 8. Comparison of the apparent modulus of the reinforcement groups pre- and post-alkaline exposure.

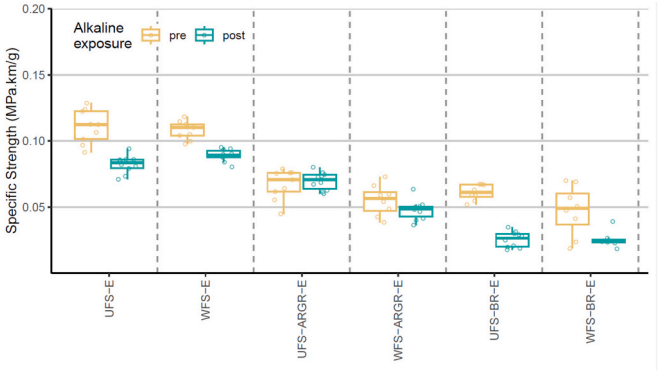

Fig. 9. Comparisons of the apparent tensile strength of the reinforcement groups pre- and post-alkaline exposure.

performances than the WFS hybrids.

3.2.3. *Bond between the flax and hybrid meshes and the surrounding cementitious matrix*

The typical force-displacement diagrams recorded during the pull-out tests are presented Fig. 10. The pull-out process can be divided in 3 phases according to Redon et al. [33]. The first phase corresponds to the pull out of the embedded length, whose end is not moving, with a constant displacement, resulting in an increasing pull-out force. In this phase, the deformation of the mesh corresponds to the elastic deformation of the debonded part and the free length [33]. At the end of phase 1, the maximum force of the curves is obtained and used to calculate the corresponding average bonding strengths (reported Fig. 11). In the second phase, as the bond between the mesh and the cementitious matrix breaks, the pull-out force drops substantially. In the third phase, the mesh is fully debonded and the embedded end starts to slide in the pull-out direction. The resulting load in this third sliding phase is caused by frictional forces. In our case, complete pull-out of the meshes from the matrix was not possible due to the free mesh end and the meshes were, therefore, pulled through the cementitious matrix.

Curves associated with the debonding of flax-based meshes (UFS-E and WFS-E) most often resulted in an abrupt failure corresponding to a sudden pull-out of the tread, with a quasi inexistant slipping phase. This can be explained by their more circular cross-section (see Fig. 6) than the hybrid meshes. Indeed, when the bond with the cementitious matrix breaks, the constant diameter of the mesh allows it to slide without recording any friction. On the contrary, hybrid reinforcements displayed a gradual decline in the slipping phase, also called slip-softening phenomenon, due to the irregularity of their cross-section (Fig. 6). On average, in the case of the flax meshes, the failure occurred at higher displacements (2–3 times higher) compared to the failure associated with the hybrid meshes. Given that the elongation at break of the flax and hybrid meshes were found in the same range (see Table 6), this observation was interpreted as sign of better bonding of the flax meshes with the cementitious matrix. The superior bonding strength for the flax

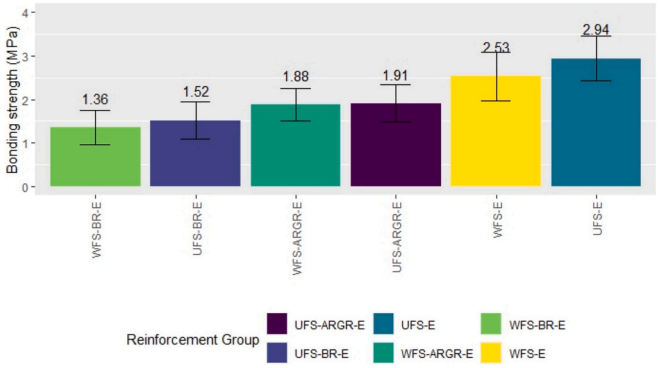

Fig. 11. Comparisons of the bonding strength between each type of reinforcement group and a high-performance concrete matrix.

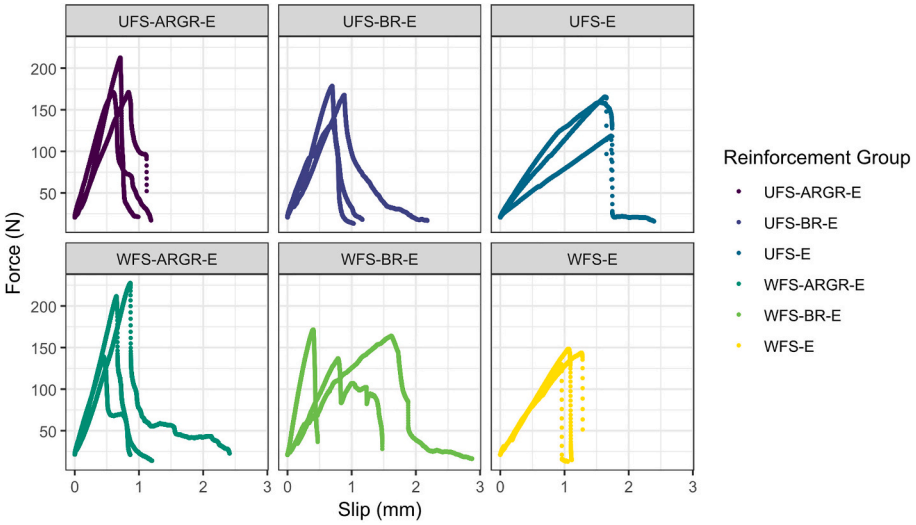

Fig. 10. Typical pullout force displacement diagrams for reinforcement groups.

meshes was confirmed (Fig. 11), with average values at 2.53 and 2.94 MPa for WFS-E and UFS-E, respectively. Hybrids in combination with glass fibres displayed similar bonding strengths at 1.88 and 1.91 MPa for WFS-ARGR-E and UFS-ARGR-E, respectively. Hybrids in combination with basalt fibres displayed the lowest bonding strengths at 1.36 and 1.52 MPa for WFS-BR-E and UFS-BR-E, respectively. Attia et al. [34] compared the bonding strength of fibre reinforced polymers made of glass and flax pulled out from different cementitious matrices (normal-strength, high-strength concrete, and ultra-high performance concrete). The compressive strength of their ultra-high performance concrete (128.23 MPa [34]) is close to the one used in this study (140.5 MPa reported by Vlach et al. [24]). With a bar diameter of 12 mm using polyester thermoset resin as the polymer (vs epoxy in this study), Attia et al. [34] obtained bond strengths in the same magnitude as this study, with 9.32 MPa and 1.32 MPa for the glass fibres bars and the flax fibres bars, respectively, pulled out of the ultra-high performance concrete matrix. However, in the case of the flax bars, the authors [34] observed a failure due to a rupture of the bars near the edge of the concrete, which they attributed to the bond strength between the bars and the concrete being higher than the tensile strength of the bars. Comparison of bond strength values with available literature are difficult because many parameters are influencing: the material and structure of the fibre/mesh/bar reinforcement, the polymer fibre/volume fraction, the surface roughness, the diameter, the anchorage length, the compressive performances of the cementitious matrix, to cite a few [33–35].

In this study, all the meshes are embedded in the same epoxy matrix, so the chemical bonding with the cementitious matrix is assumed to be similar for all the reinforcements. Hence, the observed differences in bonding were attributed to two main parameters: 1) the mechanical anchoring by embossments or undercuts resulting from the meshes roughness. In comparison with flax strands which contain single fibres sticking out creating additional bumps, the smoother surfaces of the basalt and glass rovings conducted to an overall diminished roughness of the hybrid meshes, resulting in lower bonding strengths. 2) the initial differences in cross section area between the reinforcement groups. Indeed, Liao et al. [35] highlighted a decrease in bond strength associated with greater bar diameter. Similarly, in this study, the bond strength tended to decrease for the reinforcement groups with the higher cross section (Table 3).

4. Conclusions

Flax based meshes were developed as basic components for a reinforcement grid in cementitious materials. Flax strands and hybrid strands (combination of flax strands and glass or basalt rovings) were impregnated with an epoxy resin to form the meshes. The density and the linear density of the reinforcement groups (strands and meshes) were evaluated. The density of the two flax strands was measured at 1.54 g/cm^3 and 1.69 g/cm^3 respectively, which are more than 50 % lower than the density of the synthetic glass and basalt fibres. These results highlight the necessity of considering the linear density of the reinforcements groups and their associated cross-sectional area when calculating the mechanical properties. Despite the close cross-section results provided by the two measurements methods, the images obtained by the fingerprint method revealed the irregular cross section shape of the hybrid meshes and, therefore, are considered more accurate. Hence, the cross-sectional area obtained by the fingerprint method was used to calculate the tensile strength and Young's modulus for the comparison of the mechanical properties.

At isoweight of reinforcement, the flax-based meshes demonstrated the best performance in terms of specific modulus and specific strength compared to the hybrid meshes. The control untreated UFS-E with the lowest linear density outperformed the control WFS-E. However, after alkaline exposure, the specific tensile properties of both flax-based meshes were comparable due to a greater loss of performance observed in the untreated flax. Since the WFS underwent a bleaching treatment, a part of its constituents (pectins, hemicelluloses and lignin) was already removed prior to the alkaline exposure, which explains why the WFS-E was less affected than UFS-E. Hence, we recommend the use of bleached flax strands for fabricating flax-based meshes, but with a linear density equivalent to the one of UFS.

At isoweight, the hybrid meshes from the control batch displayed specific properties in the same range, whether they were constituted of AR-glass or basalt. However, the use of alkali-resistant glass rovings strongly mitigated the degradation of the mechanical properties of the hybrids meshes by making them less affected by the alkaline environment, among all the reinforcement meshes. In contrast, hybrid meshes with basalt experienced an extensive reduction in tensile strength and strain after exposure to alkaline environment, due to the corrosion of the basalt fibres.

Pull-out tests revealed maximum bond strengths for the flax based meshes embedded in a high-performance concrete matrix. The bond strengths of the reinforcement were controlled by the mechanical anchoring resulting from the meshes roughness. And the initial differences in cross section area between the reinforcement groups.

The study highlighted that, from a mechanical point of view and considering durability aspects, flax based meshes and hybrid flax/AR-glass meshes impregnated with epoxy displayed promising performances for developing more sustainable reinforcements for cementitious materials. Yet, the slight loss of mechanical performances of these reinforcements following the alkaline exposure questions their long-term durability in concrete. A future study will investigate the development of TRC using flax based meshes and hybrid flax/AR-glass meshes and assess their immediate and long-term mechanical properties through accelerated ageing including humidity cycles and freeze-thaw tests. In addition, the replacement of epoxy with more environmentally friendly binders will be explored.

CRediT authorship contribution statement

Jaka Gašper Pečnik: Writing – review & editing, Writing – original draft, Investigation, Data curation, Conceptualization, Visualization, Formal analysis. **Laetitia Marrot:** Conceptualization, Supervision, Writing – review & editing, Funding acquisition. **Marica Mikuljan:** Conceptualization, Investigation, Methodology. **Tania Langella:** Investigation. **Matthew Schwarzkopf:** Project administration, Conceptualization, Resources.

Funding sources

Authors gratefully thank and acknowledge funding from the Slovenian Research and Innovation Agency (ARIS) for funding research projects N2-0225, J4-4546, N2-0280, and J4-50132. Additionally they acknowledge funding of ARIS for research program P4-0459 and infrastructure funding IO-0035. They also thank the Republic of Slovenia (Investment funding of the Republic of Slovenia and the European Regional Development Fund) and the European Commission for funding the InnoRenew project (Grant Agreement #739574) under the Horizon Widespread-Teaming program and the FRISSBE project (Grant Agreement #952395) under the Horizon 2020 Research and Innovation programme.

Declaration of competing interest

The authors declare that they have no known competing financial interests or personal relationships that could have appeared to influence the work reported in this paper.

Data availability

Data will be made available on request.

References

[1] Global Cement, Concrete Association, Cement Industry Net Zero Progress Report 2024/25 [Online]. Available: https://gccassociation.org/wp-content/uploads/2024/11/GCCA-Cement-Industry-Progress-Report-202425.pdf, 2025.

[2] A. Adesina, Recent advances in the concrete industry to reduce its carbon dioxide emissions, Environ. Challeng. 1 (Dec. 2020) 100004, https://doi.org/10.1016/j.envc.2020.100004.

[3] F. Leonhardt, Cracks and crack control in concrete structures, PCIJ 33 (4) (Jul. 1988) 124–145, https://doi.org/10.15554/pcij.07011988.124.145.

[4] W. Brameshuber, Report 36: Textile Reinforced Concrete - State-of-the-Art Report of RILEM TC 201-TRC, RILEM Publications, 2006.

[5] M. Curbach, et al., Sachstandbericht zum Einsatz von Textilien im Massivbau, Kurzberichte Aus Der Bauforschung 40 (1) (1999). Accessed: Apr. 01, 2020. [Online]. Available: https://trid.trb.org/view/963177.

[6] A. Peled, A. Bentur, B. Mobasher, Textile Reinforced Concrete, 1 edition, CRC Press, Boca Raton, 2017.

[7] R. Li, M. Deng, L. Guo, D. Wei, Y. Zhang, T. Li, Tensile behavior of high-strength highly ductile fiber-reinforced concrete with embedded carbon textile grids, Construct. Build Mater. 414 (Feb. 2024) 134957, https://doi.org/10.1016/j.conbuildmat.2024.134957.

[8] S. Paul, R. Gettu, D. Naidu Arnepalli, R. Samanthula, Experimental evaluation of the durability of glass textile-reinforced concrete, Construct. Build Mater. 406 (Nov. 2023) 133390, https://doi.org/10.1016/j.conbuildmat.2023.133390.

[9] G. Vandereecken, C. Toderascu, M. El Kadi, D. Van Hemelrijck, T. Tysmans, Influence of coating and reinforcement volume fraction on woven basalt TRC: an experimental study, Construct. Build Mater. 444 (Sep. 2024) 137740, https://doi.org/10.1016/j.conbuildmat.2024.137740.

[10] A. Bourmaud, J. Beaugrand, D.U. Shah, V. Placet, C. Baley, Towards the design of high-performance plant fibre composites, Prog. Mater. Sci. 97 (Aug. 2018) 347–408, https://doi.org/10.1016/j.pmatsci.2018.05.005.

[11] D. Asprone, M. Durante, A. Prota, G. Manfredi, Potential of structural pozzolanic matrix–hemp fiber grid composites, Construct. Build Mater. 25 (6) (Jun. 2011) 2867–2874, https://doi.org/10.1016/j.conbuildmat.2010.12.046.

[12] A. Hakamy, F.U.A. Shaikh, I.M. Low, Thermal and mechanical properties of NaOH treated hemp fabric and calcined nanoclay-reinforced cement nanocomposites, Mater. Des. 80 (Sep. 2015) 70–81, https://doi.org/10.1016/j.matdes.2015.05.003.

[13] A. Hakamy, F. Shaikh, I.M. Low, Microstructures and mechanical properties of hemp fabric reinforced organoclay–cement nanocomposites, Construct. Build Mater. 49 (Dec. 2013) 298–307, https://doi.org/10.1016/j.conbuildmat.2013.08.028.

[14] H. Assaedi, T. Alomayri, F.U.A. Shaikh, I.-M. Low, Characterisation of mechanical and thermal properties in flax fabric reinforced geopolymer composites, J. Adv. Ceram. 4 (4) (Dec. 2015) 272–281, https://doi.org/10.1007/s40145-015-0161-1.

[15] M. Fidelis, F. Silva, R. Toledo Filho, The influence of Fiber treatment on the mechanical behavior of jute textile reinforced concrete, Key Eng. Mater. 600 (Apr. 2014), https://doi.org/10.4028/www.scientific.net/KEM.600.469.

[16] W. Ma, L. Yan, B. Kasal, Bond and tensile properties of flax textile reinforced recycled aggregate concrete: strategies for interfacial enhancement and corresponding mechanisms, Case Stud. Constr. Mater. 21 (Dec. 2024) e04006, https://doi.org/10.1016/j.cscm.2024.e04006.

[17] H.-E. Gram, Durability of natural fibres in concrete, Swedish Cement Concrete Res Inst 225 (1983). Accessed: Dec. 03, 2024. [Online]. Available: https://urn.kb.se/resolve?urn=urn:nbn:se:ri:diva-2874.

[18] F. Majstorović, V. Sebera, M. Mrak, S. Dolenec, M. Wolf, L. Marrot, Impact of metakaolin on mechanical performance of flax textile-reinforced cement-based composites, Cement Concr. Compos. 126 (Feb. 2022) 104367, https://doi.org/10.1016/j.cemconcomp.2021.104367.

[19] A.J. Majumdar, J.F. Ryder, Glass fibre reinforcement of cement products, Glass Technol. 9 (1968) 78–84.

[20] V. Fiore, T. Scalici, G. Di Bella, A. Valenza, A review on basalt fibre and its composites, Compos. Part B Eng. 74 (Jun. 2015) 74–94, https://doi.org/10.1016/j.compositesb.2014.12.034.

[21] C. Zhou, S.Q. Shi, Z. Chen, L. Cai, L. Smith, Comparative environmental life cycle assessment of fiber reinforced cement panel between kenaf and glass fibers, J. Clean. Prod. 200 (Nov. 2018) 196–204, https://doi.org/10.1016/j.jclepro.2018.07.200.

[22] I. Merta, A. Mladenovič, J. Turk, A. Šajna, A.M. Pranjić, Life cycle assessment of natural fibre reinforced cementitious composites, Key Eng. Mater. 761 (2018) 204–209, https://doi.org/10.4028/www.scientific.net/KEM.761.204.

[23] J. Ding, et al., The physiochemical alteration of flax fibers structuring components after different scouring and bleaching treatments, Ind. Crops Prod. 160 (Feb. 2021) 113112, https://doi.org/10.1016/j.indcrop.2020.113112.

[24] T. Vlach, J. Řepka, J. Hájek, R. Fürst, Z. Jirkalová, P. Hájek, Cohesion test of a single impregnated ar-glass roving in high-performance concrete, Civil Eng. J. 29 (3) (Oct. 2020) 3, https://doi.org/10.14311/CEJ.2020.03.0032.

[25] M. Le Gall, P. Davies, N. Martin, C. Baley, Recommended flax fibre density values for composite property predictions, Ind. Crop. Prod. 114 (Apr. 2018) 52–58, https://doi.org/10.1016/j.indcrop.2018.01.065.

[26] V. Fiore, G. Di Bella, A. Valenza, Glass–basalt/epoxy hybrid composites for marine applications, Mater. Des. 32 (4) (Apr. 2011) 2091–2099, https://doi.org/10.1016/j.matdes.2010.11.043.

[27] E. Richely, et al., Influence of defects on the tensile behaviour of flax fibres: cellulose microfibrils evolution by synchrotron X-ray diffraction and finite element modelling, Composites C 9 (Oct. 2022) 100300, https://doi.org/10.1016/j.jcomc.2022.100300.

[28] L. Marrot, A. Bourmaud, P. Bono, C. Baley, Multi-scale study of the adhesion between flax fibers and biobased thermoset matrices, Mater. Des. 62 (Oct. 2014) 47–56, https://doi.org/10.1016/j.matdes.2014.04.087.

[29] A.M. Amaro, P.N.B. Reis, M.A. Neto, C. Louro, Effects of alkaline and acid solutions on glass/epoxy composites, Polym. Degrad. Stab. 98 (4) (Apr. 2013) 853–862, https://doi.org/10.1016/j.polymdegradstab.2012.12.029.

[30] J.A. de Melo Filho, F.A. de Silva, R.D. Toledo Filho, Degradation kinetics and aging mechanisms on sisal fiber cement composite systems, Cem. Concr. Compos. 40 (Jul. 2013) 30–39, https://doi.org/10.1016/j.cemconcomp.2013.04.003.

[31] M. Liu, et al., Investigation into the long-term alkali resistance of basalt fibers, J. Build. Eng. 98 (Dec. 2024) 111105, https://doi.org/10.1016/j.jobe.2024.111105.

[32] D. Xing, X.-Y. Xi, P.-C. Ma, Factors governing the tensile strength of basalt fibre, Compos. A: Appl. Sci. Manuf. 119 (Apr. 2019) 127–133, https://doi.org/10.1016/j.compositesa.2019.01.027.

[33] C. Redon, V.C. Li, C. Wu, H. Hoshiro, T. Saito, A. Ogawa, Measuring and modifying Interface properties of PVA fibers in ECC matrix, J. Mater. Civ. Eng. 13 (6) (Dec. 2001) 399–406, https://doi.org/10.1061/(ASCE)0899-1561(2001)13:6(399).

[34] M.M. Attia, M.M. Olwan, E. Amoush, S.R.R.H. Aamer, M.A. Eita, Behavior of hybrid natural fiber reinforced polymers bars under uniaxial tensile strength and pull-out loads with UHPC, Case Stud. Constr. Mater. 21 (Dec. 2024) e03442, https://doi.org/10.1016/j.cscm.2024.e03442.

[35] J. Liao, J.-J. Zeng, Y.-L. Bai, L. Zhang, Bond strength of GFRP bars to high strength and ultra-high strength fiber reinforced seawater sea-sand concrete (SSC), Compos. Struct. 281 (2022) 115013, https://doi.org/10.1016/j.compstruct.2021.115013.